Wrap–bake–peel process for nanostructural transformation from β-FeOOH nanorods to biocompatible iron oxide nanocapsules

YUANZHE PIAO[1], JAEYUN KIM[1], HYON BIN NA[1], DOKYOON KIM[1], JI SEON BAEK[2], MI KYEONG KO[2], JUNG HEE LEE[2], MOHAMMADREZA SHOKOUHIMEHR[1] AND TAEGHWAN HYEON[1]*

[1]National Creative Research Initiative Center for Oxide Nanocrystalline Materials and School of Chemical and Biological Engineering, Seoul National University, Seoul 151-744, South Korea

[2]Department of Radiology, Samsung Medical Center, Sungkyunkwan University School of Medicine, Seoul 135-710, South Korea

*e-mail: thyeon@snu.ac.kr

Published online: 17 February 2008; doi:10.1038/nmat2118

The thermal treatment of nanostructured materials to improve their properties generally results in undesirable aggregation and sintering. Here, we report on a novel wrap–bake–peel process, which involves silica coating, heat treatment and finally the removal of the silica layer, to transform the phases and structures of nanostructured materials while preserving their nanostructural characteristics. We demonstrate, as a proof-of-concept, the fabrication of water-dispersible and biocompatible hollow iron oxide nanocapsules by applying this wrap–bake–peel process to spindle-shaped akagenite (β-FeOOH) nanoparticles. Depending on the heat treatment conditions, hollow nanocapsules of either haematite or magnetite were produced. The synthesized water-dispersible magnetite nanocapsules were successfully used not only as a drug-delivery vehicle, but also as a T_2 magnetic resonance imaging contrast agent. The current process is generally applicable, and was used to transform heterostructured FePt nanoparticles to high-temperature face-centred-tetragonal-phase FePt alloy nanocrystals.

Thermal treatment is routinely used to induce transformations of phases and structures and to improve the properties of various materials[1–3]. For nanostructured materials, however, annealing at high temperature usually leads to undesirable aggregation and sintering[4–7], thus causing them to lose their nanostructural characteristics. Here, we introduce a novel wrap–bake–peel process to induce the transformation of the phases and structures of nanostructured materials while preserving their nanostructural characteristics. We demonstrate, as a proof-of-concept, the fabrication of water-dispersible and biocompatible hollow iron oxide nanocrystals. Hollow nanostructured materials have attracted tremendous attention from researchers in various disciplines for their many technological applications, because various functional materials can be incorporated into their hollow interior. Many hollow-structured nanomaterials of metals[8–11], metal oxides[12] and other materials[13–17] have been synthesized using various procedures, including the most popular template approach. Iron oxide nanomaterials are of great interest, because of their use in diverse areas. Nanomaterials of haematite (α-Fe_2O_3, the most stable form of iron oxide under ambient conditions) have been applied to gas sensors[18], catalysts[19] and electrode materials[20]. Magnetic iron oxide nanomaterials (Fe_3O_4 and γ-Fe_2O_3) have been studied for various biomedical applications including magnetic resonance imaging (MRI) contrast agents, magnetic-guided drug-delivery vehicles and the magnetic separation of biological materials[21–27]. Recently, hollow iron oxide nanostructured materials have been fabricated using various synthetic routes[28–31]. However, most of them are unsuitable for biomedical applications because of their poor water-dispersibility, which is derived from their large particle size or hydrophobic nature. Here, we report on the fabrication of water-dispersible hollow iron oxide (haematite and magnetite) nanocapsules from the nanostructural transformation of readily synthesized β-FeOOH nanoparticles. Furthermore, we also demonstrate that the magnetite nanocapsules can be used not only as a novel controlled-release drug-delivery vehicle, but also as an MRI contrast agent.

The overall nanostructural transformation process is composed of (1) the wrapping of β-FeOOH nanoparticles with a silica coating, (2) heat treatment and (3) the etching of the silica layer to produce hollow iron oxide nanocapsules (Fig. 1). The detailed experimental procedure is described in the Supplementary Information. The spindle-shaped akagenite (β-FeOOH) nanoparticles were obtained from the hydrolysis of diluted aqueous iron chloride ($FeCl_3 \cdot 6H_2O$) solution[32]. A thin silica shell is then coated on each nanoparticle by a previously reported method with a slight modification[33] to obtain the β-FeOOH/silica core–shell nanostructure. The as-prepared β-FeOOH/silica nanostructure is calcined in air to form a hollow haematite nanostructure coated with a silica shell. To prepare the magnetite nanocapsules, the air-calcined sample is further heat treated under a H_2 flow. Finally, the silica shell is etched away by sonicating the sample in NaOH solution. The iron oxide nanocapsules are isolated by centrifugation and washing several times with deionized water.

During hydrolysis, the colour of the aqueous iron chloride solution slowly changed from light yellow to deep brown, indicating the formation of β-FeOOH nanoparticles. A typical transmission

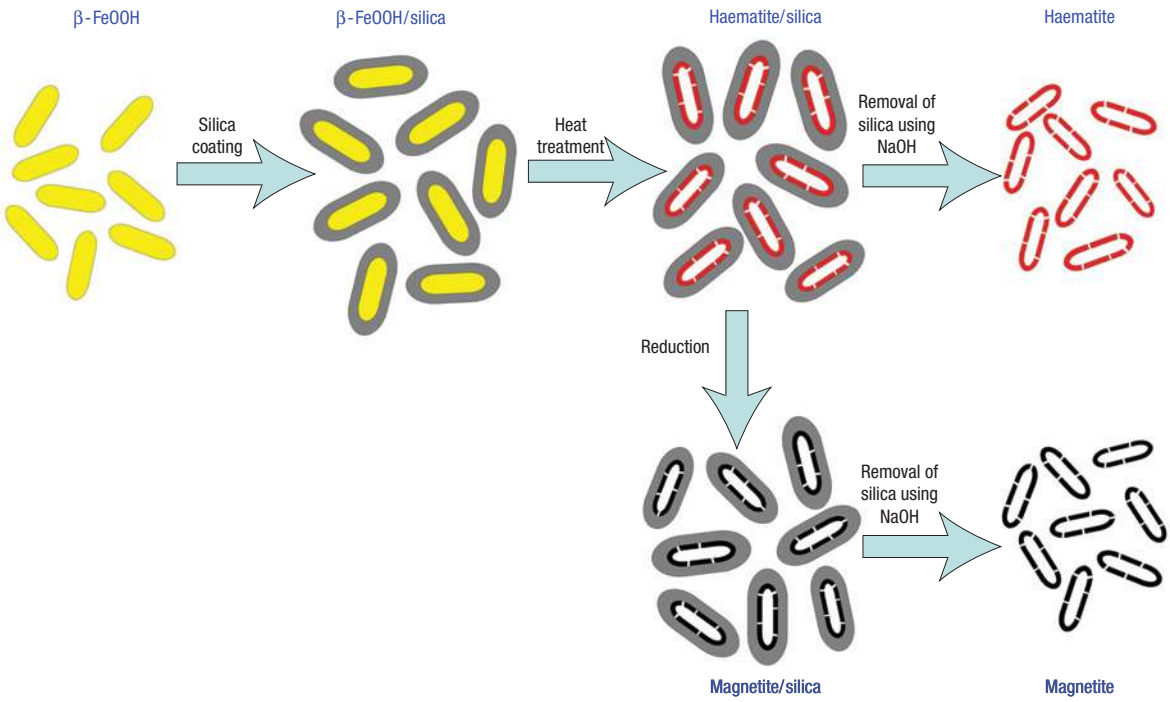

Figure 1 Schematic illustration of the procedure for the synthesis of uniform and water-dispersible iron oxide nanocapsules.

electron microscopy (TEM) image of the β-FeOOH nanoparticles, shown in Fig. 2a, reveals spindle-shaped particles with a uniform diameter of 14 ± 2 nm and length of 65 ± 8 nm (also see low-magnification TEM and scanning electron microscopy (SEM) images in Supplementary Information, Figs S1,S2). The powder X-ray diffraction (XRD) pattern reveals their β-FeOOH structure (JCPDS Card No. 75-1594) (see Supplementary Information, Fig. S3a). A thin silica shell was then coated onto each β-FeOOH nanoparticle to obtain β-FeOOH/silica nanostructures. The TEM image (Fig. 2b) confirms the formation of a uniform thin coating of silica on the β-FeOOH nanoparticles with a thickness of about 10 nm (also see low-magnification TEM and SEM images in Supplementary Information, Figs S4,S5). After isolating the silica-coated β-FeOOH nanoparticles by centrifugation and washing, heat treatment was carried out in air. The morphology change during the heat treatment process was monitored as a function of temperature. The spindle-shaped β-FeOOH nanoparticles retained their shapes after being heated at 150 °C for 5 h. After annealing at 300 °C for 5 h, irregular-shaped small pores were created inside the iron oxide nanoparticles (see Supplementary Information, Fig. S6). After heating at an increased temperature of 500 °C for 5 h, the inner iron oxide became almost entirely hollow, as illustrated in Fig. 2c. The removal of the silica coating produced hollow iron oxide nanocapsules. The resulting nanocapsule powder was readily dispersible in water, affording a transparent reddish brown suspension of well-dispersed nanoparticles (Fig. 2d, inset). The TEM image of the hollow iron oxide nanocapsules shows that they are uniform with a diameter of 14 nm, length of 65 nm and shell thickness of ~5 nm (Fig. 2d and Supplementary Information, Fig. S7). The XRD pattern of the nanocapsules reveals that they have a rhombohedral haematite (α-Fe_2O_3) structure (JCPDS Card No. 33-0664) (see Supplementary Information, Fig. S3b). The high-resolution TEM (HRTEM) images (Fig. 2e,f) confirm the highly crystalline nature of the iron oxide shell with a d-spacing value of 0.274 nm, which matches very well with d_{104}.

To understand the formation mechanism of hollow iron oxide nanocapsules, we carried out thermogravimetric analysis and differential thermal analysis of the silica-coated β-FeOOH nanorods, and we obtained TEM images after heating them at various temperatures. The thermogravimetric analysis and differential thermal analysis data showed that major weight loss and a simultaneous endothermal process occurred from 160 to 330 °C, demonstrating that thermal dehydroxylation of β-FeOOH takes place at this temperature range (see Supplementary Information, Fig. S8) (ref. 34). TEM images obtained after heating the silica-coated β-FeOOH nanorods at various temperatures showed that the small-sized pores generated at a low temperature of $\leq$200 °C were merged to form single large pore, leading to the generation of a nanocapsule structure (see Supplementary Information, Fig. S6). TEM images after annealing at $\geq$300 °C revealed that the outer surface of the hollow iron oxide nanocapsules was adhered to the inner surface of the silica shell[35]. According to previous reports on the synthesis of nanotubes using anodic alumina as a template by Gösele and co-workers, the interaction between the inner alumina wall and the material in the cylindrical nanopores during the annealing process induced the adhesion of the material, forming tubular structures[34,36]. When the β-FeOOH nanoparticles without a silica coating were heated above 300 °C, the pores generated at the lower temperature started to collapse, resulting in shrinkage of the nanoparticles, and finally leading to extensive agglomeration of the nanoparticles to form micrometre-sized ill-shaped pieces after heating at 550 °C (see Supplementary Information, Fig. S9). These results demonstrated that the coated silica shell served not only to prevent aggregation of the core nanoparticles but also to prevent the collapse of pores, generating hollow nanocapsule structures. Consequently, we speculated that the formation of the hollow nanostructures is due to the volume reduction from the

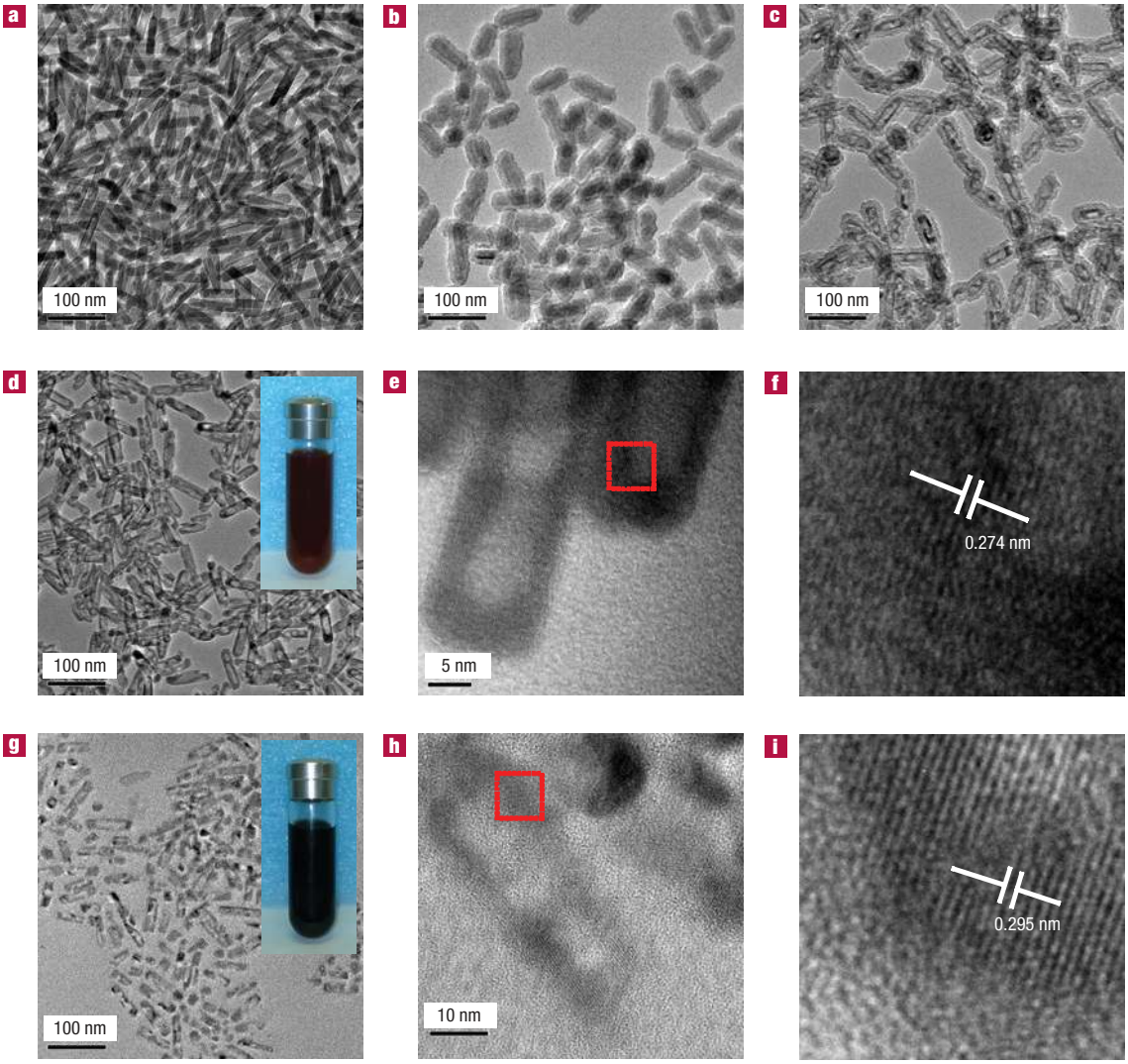

Figure 2 TEM images of each product. a, β-FeOOH nanoparticles. **b**, Silica-coated β-FeOOH nanoparticles. **c**, Iron oxide/silica nanocomposite after calcination at 500 °C for 5 h. **d**, Iron oxide nanocapsules after removal of silica shell. Inset: Photograph of the iron oxide nanocapsule solution. **e**, Higher-magnification TEM image of the iron oxide nanocapsules shown in **d**. **f**, HRTEM image of the selected area in **e**. **g**, Reduced iron oxide nanocapsules after removal of silica shell. Inset: Photograph of the iron oxide nanocapsule solution. **h**, Higher-magnification TEM image of the iron oxide nanocapsules shown in **g**. **i**, HRTEM image of the selected area in **h**. SEM images and further TEM images of each product are given in Supplementary Information, Figs S1–S9.

transformation of β-FeOOH with a low density of 3 g cm^{-3} to denser haematite with a density of 5.3 g cm^{-3} and the interaction of the outer surface of iron oxide with the inner surface of the silicon oxide shell[37].

To synthesize magnetite nanoparticles, the haematite/silica nanostructure, which was obtained after calcination of the β-FeOOH/silica nanostructure in air, was further heated under H_2 flow. The colour of the powder changed from dark red–brown to black during the reduction process (see Supplementary Information, Fig. S10). The removal of the silica layer by treating the sample with NaOH generated magnetite nanocapsules. These nanocapsules are more hollow than the haematite nanocapsules and some of them have cracks and holes in their walls (Fig. 2g). The low-magnification TEM image (Fig. 2g) shows the capsule-shaped iron oxide nanomaterials and the HRTEM image also reveals the hollow interior and crystalline wall with a d-spacing value of 0.295 nm, which matches with d_{220}. The resulting nanocapsule powder was readily dispersible in water, affording a transparent black suspension (Fig. 2g, inset). The XRD pattern of the magnetic iron oxide nanocapsules (see Supplementary Information, Fig. S3c) shows that the powder is predominantly face-centred-cubic magnetite (Fe_3O_4) phase (JCPDS Card No. 19-0629) with a small fraction of body-centred-cubic α-Fe. The broad peaks clearly demonstrate the nanoscale wall thickness of the nanocapsules.

The representative nitrogen adsorption/desorption isotherms and the corresponding pore size distribution obtained from the analysis of the adsorption branch using the Barett–Joyner–Halenda method are shown in Supplementary Information Fig. S11. The N_2 adsorption/desorption isotherms of the hollow nanocapsules of haematite and magnetite showed a major capillary condensation step at relatively high pressures of over $\sim 0.8 P/P_0$, demonstrating the presence of well-developed nanopores with a diameter of >10 nm. The Brunauer–Emmett–Teller surface areas of the β-FeOOH nanorods, haematite nanocapsules and magnetite

nanocapsules were measured to be 82.3, 165 and 171 $m^2 g^{-1}$, respectively (see Supplementary Information, Fig. S11). The total pore volumes of the β-FeOOH nanorods, haematite nanocapsules and magnetite nanocapsules were determined to be 0.30, 0.40 and 0.41 $cm^3 g^{-1}$, respectively. The pore sizes of the haematite nanocapsules and magnetite nanocapsules obtained from the analysis of the adsorption branch using the Barett–Joyner–Halenda method were centred at ∼15 nm (see Supplementary Information, Fig. S12).

The field-dependent magnetism of the as-prepared magnetite nanocapsules at 300 K showed no hysteresis (see Supplementary Information, Fig. S13), demonstrating their superparamagnetic characteristics, which are desirable for various biomedical applications. On the other hand, the β-FeOOH nanorods and haematite nanocapsules exhibited weak paramagnetic behaviour (see Supplementary Information, Figs S14,S15). One of the remarkable characteristics of the nanocapsules of both haematite and magnetite is their excellent water-dispersibility, which is the key to their successful use in biomedical applications. The as-prepared nanocapsules can completely pass through a 0.2 μm membrane filter, confirming the absence of any aggregation, and their aqueous dispersion is highly stable in water against aggregation for more than 6 months without the addition of any stabilizing reagent. The Fourier-transform infrared spectrum of the iron oxide nanocapsules (see Supplementary Information, Fig. S16) showed a band at 1,580 cm^{-1}, demonstrating the presence of oxygen-containing functional groups, which seems to be responsible for their hydrophilicity. Superparamagnetic iron oxide nanoparticles have been used as T_2 MRI contrast agents[22]. Consequently, we carried out MRI experiments on the magnetite nanocapsules. The magnetic resonance images of the poly(ethylene glycol) (PEG)-coated magnetite nanocapsules at various concentrations were measured using a 3.0 T human clinical MRI system. Figure 3a shows the T_2-weighted magnetic resonance images of the magnetite nanocapsules dispersed in water. Furthermore, we also obtained *in vitro* magnetic resonance images of the magnetite nanocapsules after incubating them with ∼10^7 SKBR3 cells for 24 h (Fig. 3b). As the concentration of the magnetite nanocapsules increases, the signal intensity of the magnetic resonance image decreases, demonstrating that the magnetite nanocapsules can be used as a T_2 MRI contrast agent.

Given their water-dispersibility and hollow interior, we tested the capability of the iron oxide nanocapsules to be used as a drug-delivery vehicle. Doxorubicin (DOX), a chemotherapeutic agent[38], was used as a model drug and was incorporated into the nanocapsules. The typical DOX loadings in the PEG-coated nanocapsules of haematite and magnetite were measured to be 17.8 wt% and 28.9 wt%, respectively, corresponding to relatively high drug loadings. The cell viability measurement of SKBR-3 cells revealed that the PEG-coated magnetite nanocapsules (PEG–MNC) exhibited very low cytotoxicity up to an iron concentration of 200 μg ml^{-1} (see Supplementary Information, Fig. S17). DOX was then loaded in the PEG–MNC (PEG–MNC–DOX) and both free DOX and PEG–MNC–DOX were fed to MDA-MB-435 cancer cells. Confocal laser scanning microscopy (CLSM) was used to study the internalization of the free DOX and PEG–MNC–DOX into the cancer cells. CLSM images of the nuclei of the cancer cells were obtained after staining (blue) by Hoechst 33342 (Fig. 4c,f). As shown in Fig. 4, the intracellular distribution of PEG–MNC–DOX is different from that of free DOX. PEG–MNC–DOX was accumulated mostly in the cytoplasm, whereas free DOX was mostly found in the cell nuclei (compare the CLSM images in Fig. 4b,c with those in Fig. 4e,f; red fluorescence from DOX and blue fluorescence from Hoechst 33342 dye). These experimental results demonstrate that PEG–MNC is an efficient delivery vehicle

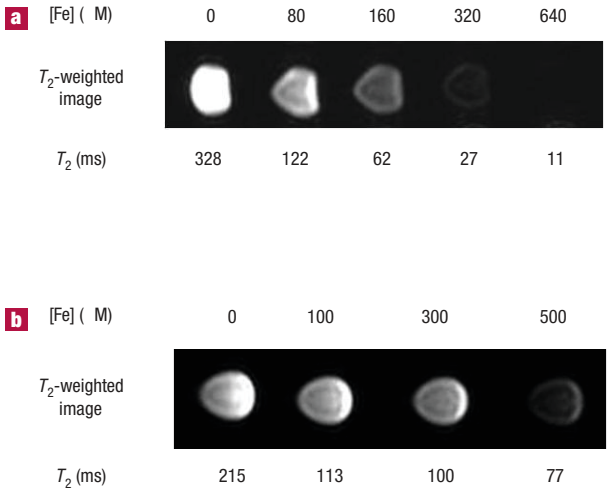

Figure 3 T_2-weighted magnetic resonance images of the magnetite nanocapsules. a, T_2-weighted magnetic resonance images of the PEG-coated magnetite nanocapsules at various concentrations in water. **b**, T_2-weighted magnetic resonance images of ∼10^7 SKBR-3 cells incubated with PEG-coated magnetite nanocapsules at various concentrations for 24 h. As the concentration of the magnetite nanocapsules increases, the signal intensity of the MR image decreases, demonstrating that the magnetite nanocapsules can be used as a T_2 MRI contrast agent.

to transport DOX to the cytoplasm via endocytosis, which is consistent with the results obtained using other nanostructured drug-delivery vehicles[39].

The delivery of DOX into the cancer cells led to growth inhibition and cell death. The *in vitro* cytotoxicity effects of free DOX and PEG–MNC–DOX were tested on SKBR-3 cancer cell lines. As shown in Fig. 4g, growth inhibition of human cancer cells was observed when the cells were treated with either free DOX or PEG–MNC–DOX, demonstrating that magnetite nanocapsules can be used as a drug-delivery vehicle. Consistent with the *in vitro* cytotoxicity and CLSM results, the entrapped DOX from PEG–MNC–DOX seems to exhibit controlled- or sustained-release behaviour.

To demonstrate the general applicability of the current wrap–bake–peel process, we synthesized face-centred-tetragonal (f.c.t.)-phase Fe–Pt alloy nanoparticles through nanostructural transformation of heterostructured FePt nanoparticles. High-temperature f.c.t.-phase Fe–Pt alloy nanocrystals have been intensively studied for their potential use as high-density magnetic storage media[5,40]. However, their synthesis turned out to be very challenging because the as-synthesized Fe–Pt alloy nanoparticles with the low-temperature face-centred-cubic phase can be readily agglomerated during the annealing process[41–45]. As shown in the TEM images (Fig. 5), the starting heterostructured FePt nanoparticles were successfully transformed into highly crystalline FePt alloy nanoparticles with a spherical shape and an average diameter of 7.2 ± 1.1 nm. The XRD patterns revealed that the starting heterostructured FePt nanoparticles were transformed into f.c.t.-phase FePt alloy nanoparticles via heat treatment at 800 °C (see Supplementary Information, Fig. S18). The resulting f.c.t. FePt alloy nanoparticles are highly dispersible in water (see Supplementary Information, Fig. S19). When we heat treated the nanoparticles without a silica coating, large particles were generated (see Supplementary Information, Figs S20,S21), demonstrating that the silica coating is crucial for obtaining water-dispersible nanoparticles.

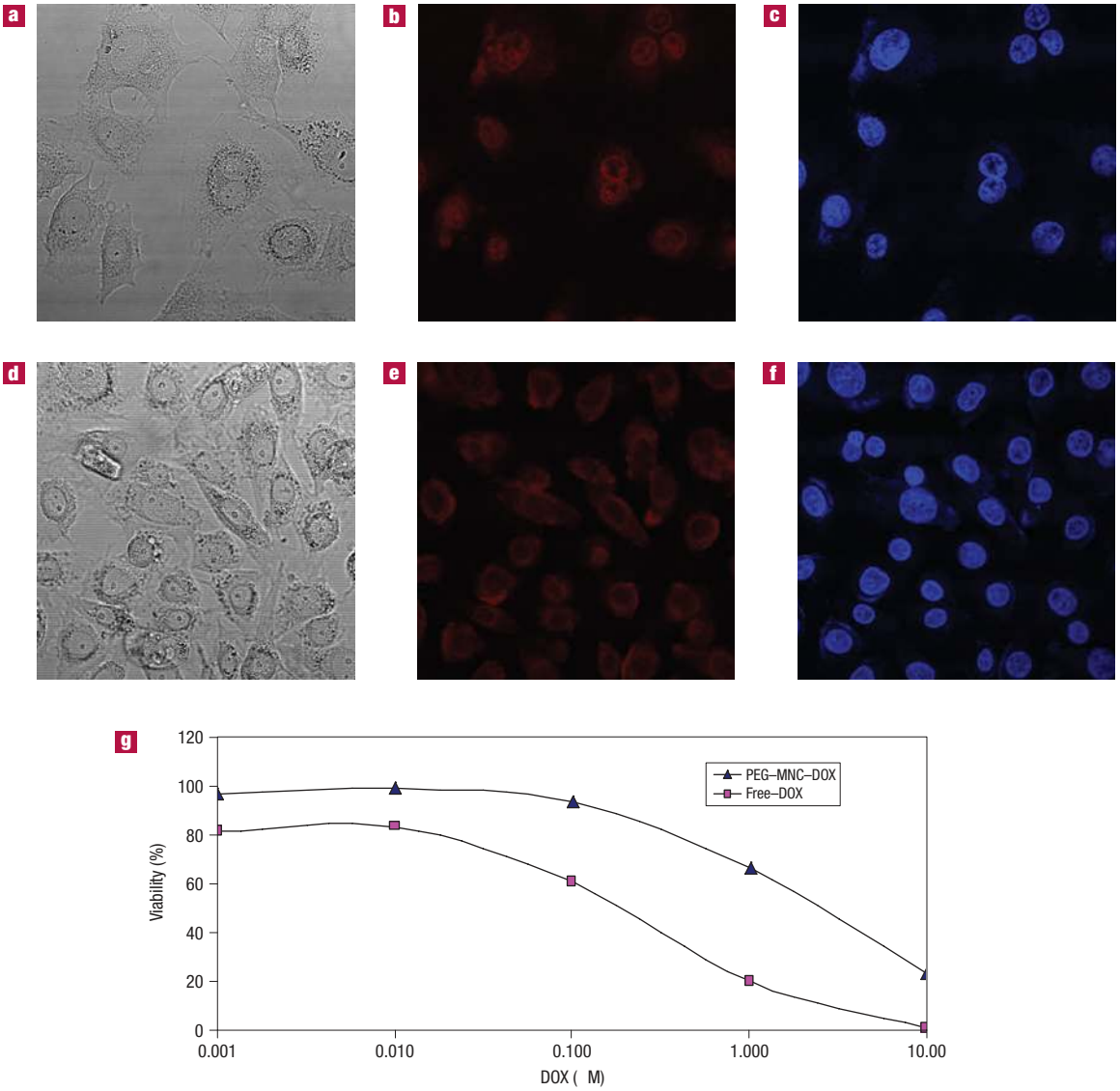

Figure 4 Uptake of free DOX and PEG–MNC–DOX in cancer cells and cytotoxicity data. The images were taken with the same exposure condition and magnification. **a**–**f**, Optical and CLSM images of free DOX incubated in MDA-MB-435 cells for 24 h (**a**–**c**) and PEG–MNC–DOX incubated in MDA-MB-435 cells for 24 h (**d**–**f**). For each row, the images from left to right show the optical microscopic image, the CLSM image of DOX fluorescence and the CLSM image of the nuclei of cells stained by Hoechst 33342. The CLSM images in **b**,**e** reveal that PEG-MNC-DOX was accumulated mostly in the cytoplasm, whereas free DOX was mostly found in the cell nuclei. **g**, *In vitro* cytotoxicity of free DOX and PEG–MNC–DOX against SKBR-3 cells, demonstrating that PEG–MNC can be used as a drug-delivery vehicle.

In summary, we developed a new general route to induce nanostructural transformation. This process is composed of silica coating/heat treatment/removal of silica (wrap–bake–peel). Water-dispersible hollow iron oxide nanocapsules were obtained by applying the wrap–bake–peel process to β-FeOOH nanoparticles. The synthesized magnetite nanocapsules could be successfully used not only as a drug-delivery vehicle, but also as a T_2 MRI contrast agent. The current process is quite general and can be used to transform heterostructured FePt nanoparticles into high-temperature f.c.t.-phase FePt alloy nanocrystals. Furthermore, this process is readily applicable to the large-scale production of biocompatible nanoparticles. For example, we were able to synthesize as much as 2 g of hollow nanocapsules of haematite and magnetite (see Supplementary Information, Fig. S22). We expect that this wrap–bake–peel process can be used for the nanostructural transformation of various kinds of material to produce many useful functional nanostructured materials.

METHODS

PREPARATION OF HAEMATITE AND MAGNETITE NANOCAPSULES

Spindle-shaped β-FeOOH nanoparticles were prepared by hydrolysis of $FeCl_3$ aqueous solution. In a typical procedure, $FeCl_3{\cdot}6H_2O$ was dissolved in 2 l of deionized water and the concentration of Fe^{3+} adjusted to 0.02 M. The solution was added to a round-bottom flask and heated at 80 °C under mechanical stirring for 12 h to obtain uniform and spindle-shaped β-FeOOH nanoparticles. The particles were isolated by centrifugation and washed with water.

Silica coating of the β-FeOOH nanoparticles was carried out using a modified version of a method reported elsewhere[33]. Briefly, 300 ml of ammonium hydroxide (30 wt%) was added to a solution containing 5 l of ethanol and 500 ml of deionized water. After being pre-coated with

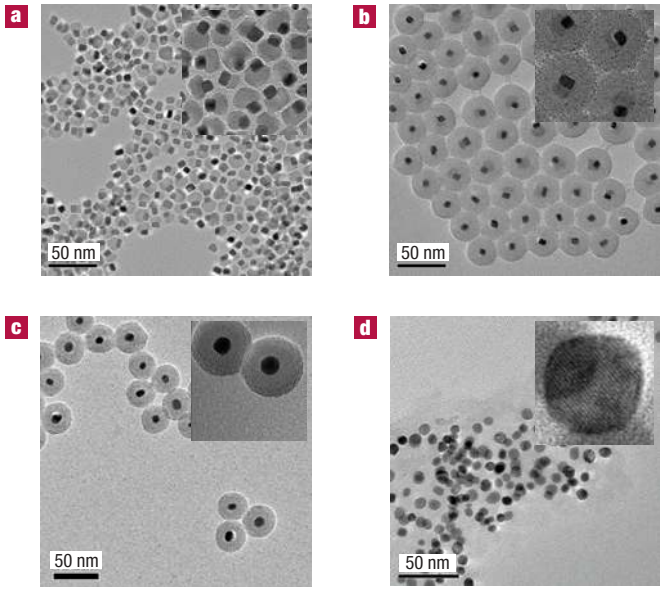

Figure 5 TEM images of each product. **a**, TEM image of the as-synthesized heterostructured FePt nanocrystals. **b**, Heterostructured FePt nanocrystals coated with silica shell. **c**, FePt/silica nanocomposite after annealing at 800 °C for 5 h under 10%/90%H_2/Ar. **d**, FePt alloy nanocrystals after removal of silica shell. The insets in each panel show higher-magnification TEM images.

polyvinylpyrrolidone, the as-prepared β-FeOOH nanoparticles were dispersed in the solution. 7 ml of tetraethoxysilane was then added to the mixture solution at room temperature with vigorous stirring. The mixture was kept at room temperature for 10 h with constant stirring to yield the uniform silica shell/β-FeOOH core nanocomposite. The nanocomposite was isolated by centrifugation and washed with water.

The composite was then heated to 500 °C under an air atmosphere and kept at this temperature for 5 h to produce the silica shell/hollow haematite nanostructures. To obtain magnetic iron oxide nanocapsules, the silica shell/hollow haematite nanostructures were further heated at 500 °C for 10 h under a flow of 10 s.c.c.m./90 s.c.c.m. H_2/Ar.

The iron oxide/silica nanostructures were immersed in 0.1 M of NaOH solution with sonication for 5 h to remove the silica shell (for 1 g of nanocomposite, 250 ml of 0.1 M NaOH was added). All of the ions in the resulting suspensions were completely removed by several cycles of centrifugation to neutral pH.

PEGYLATION OF MAGNETITE NANOCAPSULES (PEG–MNC)

2 ml of magnetite nanocapsules in water was centrifuged and redispersed in 20 ml of ethanol. 0.137 mmol of trimethoxysilyl-functionalized PEG and 300 μl of ammonium hydroxide were added to the magnetite nanocapsule solution in sequence, followed by stirring for 2 h. After centrifugation and washing with ethanol three times, the resulting PEG–MNC was redispersed in 4 ml of water (~1 mg Fe/ml).

Received 21 September 2007; accepted 9 January 2008; published 17 February 2008.

References

1. Kostorz, G. (ed.) *Phase Transformations in Materials* (Wiley-VCH, Weinheim, 2001).
2. Burstein, G. T., Hutchings, I. M. & Sasaki, K. Electrochemically induced annealing of stainless-steel surfaces. *Nature* **407**, 885–887 (2000).
3. Sundaram, S. K. & Mazur, E. Inducing and probing non-thermal transitions in semiconductors using femtosecond laser pulses. *Nature Mater.* **1**, 217–224 (2002).
4. Jacobs, K., Zaziski, D., Scher, E. C., Herhold, A. B. & Alivisatos, A. P. Activation volumes for solid-solid transformations in nanocrystals. *Science* **293**, 1803–1806 (2001).
5. Sun, S., Murray, C. B., Weller, D., Folks, L. & Moser, A. Monodisperse FePt nanoparticles and ferromagnetic FePt nanocrystal superlattices. *Science* **287**, 1989–1992 (2000).
6. Budai, J. D. *et al.* Controlling the size, structure and orientation of semiconductor nanocrystals using metastable phase recrystallization. *Nature* **390**, 384–386 (1997).
7. Zeng, H., Li, J., Liu, J. P., Wang, Z. L. & Sun, S. H. Exchange-coupled nanocomposite magnets by nanoparticle self-assembly. *Nature* **420**, 395–398 (2002).
8. Yin, Y., Erdonmez, C., Aloni, S. & Alivisatos, A. P. Faceting of nanocrystals during chemical transformation: From solid silver spheres to hollow gold octahedra. *J. Am. Chem. Soc.* **128**, 12671–12673 (2006).
9. Kim, D. *et al.* Synthesis of hollow iron nanoframes. *J. Am. Chem. Soc.* **129**, 5812–5813 (2007).
10. Liang, H.-P. *et al.* Pt hollow nanospheres: facile synthesis and enhanced electrocatalysts. *Angew. Chem. Int. Edn* **43**, 1540–1543 (2004).
11. Kim, S.-W., Kim, M., Lee, W. Y. & Hyeon, T. Fabrication of hollow palladium spheres and their successful application to the recyclable heterogeneous catalyst for suzuki coupling reactions. *J. Am. Chem. Soc.* **124**, 7642–7643 (2002).
12. Lou, X. W., Wang, Y., Yuan, C., Lee, J. Y. & Archer, L. A. Template-free synthesis of SnO_2 hollow nanostructures with high lithium storage capacity. *Adv. Mater.* **18**, 2325–2329 (2006).
13. Yin, Y. *et al.* Formation of hollow nanocrystals through the nanoscale kirkendall effect. *Science* **304**, 711–714 (2004).
14. Gasparac, R., Kohli, P., Mota, M. O., Trofin, L. & Martin, C. R. Template synthesis of nano test tubes. *Nano Lett.* **4**, 513–516 (2004).
15. Grosso, D., Boissière, C. & Sanchez, C. Ultralow-dielectric-constant optical thin films built from magnesium oxyfluoride vesicle-like hollow nanoparticles. *Nature Mater.* **6**, 572–575 (2007).
16. Dhas, N. A. & Suslick, K. S. Sonochemical preparation of hollow nanospheres and hollow nanocrystals. *J. Am. Chem. Soc.* **127**, 2368–2369 (2005).
17. Yoon, S. B. *et al.* Fabrication of carbon capsules with hollow macroporous core/mesoporous shell structures. *Adv. Mater.* **14**, 19–21 (2002).
18. Chen, J., Xu, L., Li, W. & Gou, X. α-Fe_2O_3 nanotubes in gas sensor and lithium-ion battery applications. *Adv. Mater.* **17**, 582–586 (2005).
19. Shekhah, O., Ranke, W., Schüle, A., Kolios, G. & Schlögl, R. Styrene synthesis: High conversion over unpromoted iron oxide catalysts under practical working conditions. *Angew. Chem. Int. Edn* **42**, 5760–5763 (2003).
20. Poizot, P., Laruelle, S., Grugeon, S., Dupont, L. & Tarascon, J.-M. Nano-sized transition-metal oxides as negative-electrode materials for lithium-ion batteries. *Nature* **407**, 496–499 (2000).
21. Weissleder, R., Kelly, K., Sun, E. Y., Shtatland, T. & Josephson, L. Cell-specific targeting of nanoparticles by multivalent attachment of small molecules. *Nature Biotechnol.* **23**, 1418–1423 (2005).
22. Bulte, J. W. M. & Kraitchman, D. L. Iron oxide MR contrast agents for molecular and cellular imaging. *NMR Biomed.* **17**, 484–499 (2004).
23. Xu, C. *et al.* Dopamine as a robust anchor to immobilize functional molecules on the iron oxide shell of magnetic nanoparticles. *J. Am. Chem. Soc.* **126**, 9938–9939 (2004).
24. Gu, H., Xu, K., Xu, C. & Xu, B. Biofunctional magnetic nanoparticles for protein separation and pathogen detection. *Chem. Commun.* 941–949 (2006).
25. Lee, I. S. *et al.* Ni/NiO core/shell nanoparticles for selective binding and magnetic separation of histidine-tagged proteins. *J. Am. Chem. Soc.* **128**, 10658–10659 (2006).
26. Lee, J. H. *et al.* Artificially engineered magnetic nanoparticles for ultra-sensitive molecular imaging. *Nature Med.* **13**, 95–99 (2007).
27. Son, S. J., Reichel, J., He, B., Schuchman, M. & Lee, S. B. Magnetic nanotubes for magnetic-field-assisted bioseparation, biointeraction, and drug delivery. *J. Am. Chem. Soc.* **127**, 7316–7317 (2005).
28. Jia, C.-J. *et al.* Single-crystalline iron oxide nanotubes. *Angew. Chem. Int. Edn* **44**, 4328–4333 (2005).
29. Liu, Z. *et al.* Single crystalline magnetite nanotubes. *J. Am. Chem. Soc.* **127**, 6–7 (2005).
30. Peng, S. & Sun, S. Synthesis and characterization of monodisperse hollow Fe_3O_4 nanoparticles. *Angew. Chem. Int. Edn* **46**, 4155–4158 (2007).
31. Bang, J. H. & Suslick, K. S. Sonochemical synthesis of nanosized hollow hematite. *J. Am. Chem. Soc.* **129**, 2242–2243 (2007).
32. Chen, M., Tang, B. & Nikles, D. E. Preparation of iron nanoparticles by reduction of acicular β-FeOOH particles. *IEEE Trans. Magn.* **34**, 1141–1143 (1998).
33. Graf, C., Vossen, D. L. J., Imhof, A. & van Blaaderen, A. A general method to coat colloidal particles with silica. *Langmuir* **19**, 6693–6700 (2003).
34. Steinhart, M., Wehrspohn, R. B., Gösele, U. & Wendorff, J. H. Nanotubes by template wetting: A modular assembly system. *Angew. Chem. Int. Edn* **43**, 1334–1344 (2004).
35. Bondioli, F., Ferrari, A. M., Leonelli, C. & Manfredini, T. Synthesis of Fe_2O_3/silica red inorganic inclusion pigments for ceramic applications. *Mater. Res. Bull.* **33**, 723–729 (1998).
36. Luo, Y., Lee, S. K., Hofmeister, H., Steinhart, M. & Gösele, U. Pt nanoshell tubes by template wetting. *Nano Lett.* **4**, 143–147 (2004).
37. da Silva, S. W. *et al.* Raman spectroscopy of cobalt ferrite nanocomposite in silica matrix prepared by sol–gel method. *J. Non-Cryst. Solids* **352**, 1602–1606 (2006).
38. Booser, D. J. & Hortobagyi, G. N. Anthracycline antibiotics in cancer therapy: focus on drug resistance. *Drugs* **47**, 223–258 (1994).
39. Geng, Y. *et al.* Shape effects of filaments versus spherical particles in flow and drug delivery. *Nature Nanotechnol.* **2**, 249–255 (2007).
40. Sun, S. Recent advances in chemical synthesis, self-assembly, and applications of FePt nanoparticles. *Adv. Mater.* **18**, 393–403 (2006).
41. Lee, D. C., Mikulec, F. V., Pelaez, J. M., Koo, B. & Korgel, B. A. Synthesis and magnetic properties of silica-coated FePt nanocrystals. *J. Phys. Chem. B* **110**, 11160–11166 (2006).
42. Hyun, C., Lee, D. C., Korgel, B. A. & de Lozanne, A. Micromagnetic study of single-domain FePt nanocrystals overcoated with silica. *Nanotechnology* **18**, 055704 (2007).
43. Varanda, L. C. & Jafelicci, M. Self-assembled FePt nanocrystals with large coercivity: reduction of the fcc-to-L1(0) ordering temperature. *J. Am. Chem. Soc.* **128**, 11062–11066 (2006).
44. Kang, S., Harrell, J. W. & Nikles, D. E. Reduction of the fcc to L1(0) ordering temperature for self-assembled FePt nanoparticles containing Ag. *Nano Lett.* **2**, 1033–1036 (2002).
45. Dai, Z. R., Sun, S. H. & Wang, Z. L. Phase transformation, coalescence, and twinning of monodisperse FePt nanocrystals. *Nano Lett.* **1**, 443–447 (2001).

Acknowledgements

T.H. acknowledges financial support by the Korean Ministry of Science and Technology through the National Creative Research Initiative Program of the Korea Science and Engineering Foundation (KOSEF).
Correspondence and requests for materials should be addressed to T.H.
Supplementary Information accompanies this paper on www.nature.com/naturematerials.